Nanometer-scale Phase Separation in Manganites

Sahana Rößler, Steffen Wirth, Stefan Ernst, Balasubramanian Padmanabhan[1], Suja Elizabeth[1], Handadi L. Bhat[1], and Frank Steglich

Introduction

Doped manganites have become very popular over the past 15 years since they not only exhibit rich physics and a number of extraordinary effects but may also provide many opportunities for applications [1]. The origin of the vast number of phenomena stems from an interplay of lattice, charge, orbital and spin degrees of freedom which all take place at comparable energy scales [2]. This may, along with competing long-rang interactions, give rise to phase separation (PS) [3], a rather general concept in strongly correlated electron systems. In mixed-valent manganites of perovskite type $AMnO_3$ (A–rare earth or doped divalent ion) such PS into insulating paramagnetic and conducting ferromagnetic regions has been observed by various experimental techniques, such as electron microscopy [4], scanning tunneling microscopy and spectroscopy (STM/S) [5,6], magnetic force microscopy [7] and photoelectron spectroscopy [8]. These experiments showed inhomogeneities of random shape on a length scale of several hundred nanometers. Furthermore, the PS persisted deep into the metallic low-temperature state in some of these manganites. However, computational studies on models of manganites considering double exchange, Jahn-Teller interaction and long-range Coulomb potential could show only regularly spaced nanometer-scale PS [9]. The random location and shape of the clusters observed experimentally [4–8] are conjectured to be caused by quenched disorder in the couplings induced by chemical substitution [10,11]. Recent STS studies combined with transmission electron microscopy [12] on A-site ordered and disordered thin films $La_{0.75}Ca_{0.25}MnO_3$ showed that PS persists in the metallic state only in the disordered film. But this study does not address the question of PS at the metal-insulator transition temperature, T_{MI}. Thus, the origin of the PS, the length scale involved, the role of quenched disorder originating from the random A-site substitution, and the temperature range at which PS occurs, remain strongly debated.

To address some of these issues experimentally, we carried out STM/S on $Pr_{0.68}Pb_{0.32}MnO_3$ (PPMO) single crystals. This compound has a tolerance factor of 0.97 and hence, minimum internal strain. Previously reported [5,6] STS measurements on manganites observing PS were carried out on thin film samples where substrate induced strain and the granular structure are known extrinsic sources for PS [13,14]. Moreover, the STS measurements [5] on thin films of $La_{0.73}Ca_{0.27}MnO_3$ on $SrTiO_3$, showing coexistence of regions with metallic, insulating as well as intermediate conductivities, extending over several hundred nanometers, were obtained at a rather high bias voltage $V = 3$ V (much larger than the semiconducting gap of 0.2–0.3 V in manganites) and may not reflect the ground state properties. To overcome this, Becker *et al.* mapped the zero-bias conductance, $G_0 = dI/dV|_{V=0}$, of thin films $La_{0.7}Sr_{0.3}MnO_3/MgO$ as a function of temperature T. However, they applied a threshold criterion to distinguish metallic and insulating regions [6]. Such a threshold criterion will not give an unambiguous evidence for the existence of PS because any statistical distribution of conductance, whose average value shifts with T, will seem to show PS [15]. Therefore, in order to provide clear evidence for PS, we analyze the entire distribution of G_0 *and* its dependence on T. This approach gives direct information on the length scale of the inhomogeneities and the temperature range within which it appears. In order to ensure that our observations are not *primarily* driven by surface effects, we compare the STS results with macroscopic measurements on the same single crystals. Our results are featured in a recent review [13].

Properties of $Pr_{1-x}Pb_xMnO_3$ manganites

The preparation and properties of PPMO single crystals were reported in [16,17]. In $Pr_{1-x}PbxMnO_3$, the Curie temperature T_C and T_{MI} do not coincide, and metallic conductivity occurs in the paramagnetic state in parts of the phase diagram [16,18], a phenomenon uncommon to mixed va-
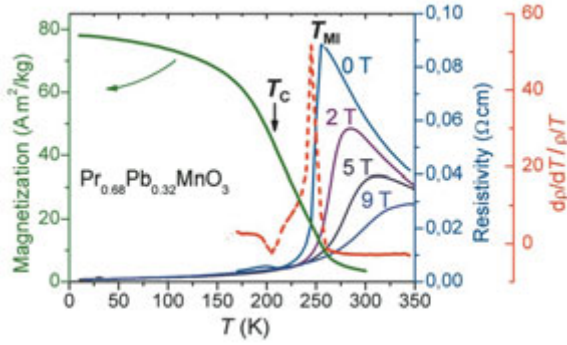
Fig. 1: Temperature dependence of magnetization (left scale) and resistivity (blue right scale) of $Pr_{0.68}Pb_{0.32}MnO_3$ single crystals measured at different magnetic fields. The red dashed line represents the logarithmic derivative of resistivity, $(d\rho/dT)/(\rho/T)$ at zero field (red right scale) indicating both T_{MI} and T_C.

lence manganites. Fig. 1 shows the temperature dependence of magnetization (M) and resistivity (ρ) at selected magnetic fields of a PPMO sample. The magnetoresistance, $[\rho(H)–\rho(0)]/\rho(0)$, is found to be about 90% close to T_{MI} and at a field of 9 T. From the maximum change in slope of the M vs. T curve, $T_C \sim 210$ K was estimated which is distinctly lower than the corresponding $T_{MI} \approx 255$ K. This kind of approach to estimate T_C is supported by elaborate investigations [17] on a similar single crystal $Pr_{0.7}Pb_{0.3}MnO_3$ in which the so-determined $T_C \sim 197$ K agrees well with results from detailed static magnetization scaling analysis ($T_{MI} \approx 235$ K in this compound [16]). The scaling analysis near the critical temperature indicated in addition that the underlying magnetic transition is a conventional one, with short-range Heisenberg-like critical exponents. This study emphasizes the presence of additional frustrated couplings which intercepts the formation of long-range order. Deviation of the susceptibility from the Curie-Weiss law above T_C [16] and history-dependent transport properties [18] suggest the presence of small magnetic metallic clusters above T_C that form percolating metallic paths in the paramagnetic metallic state upon reducing T. Note that evidence for the formation of localized ~1.2 nm magnetic clusters above T_C in another mixed valent manganite has earlier been found by small-angle neutron scattering measurements [19]. We also note the sharpness of the resistive transition which can be inferred from the logarithmic derivative of the resistivity, $(d\rho/dT)/(\rho/T)$, *cf.* Fig. 1. Such a sharp metal-insulator transition is indicative of a largely strain-free sample [14].

Scanning tunneling spectroscopy

For the tunneling studies a STM (Omicron Nanotechnology) under ultra high vacuum conditions ($p \leq 10^{-10}$ mbar) was utilized at numerous fixed temperatures, 30 K $\leq T \leq$ 300 K, mostly in the vicinity of T_C and T_{MI}. Since crystals with perovskite structure do not cleave easily, preparing a clean surface for STM studies is a challenge. Just before inserting the crystal into the UHV chamber, we scraped the surface inside isopropanol to rip off some part of it. This preparation gave locally cleaved surfaces on a length scale of micrometers. STM was conducted using tungsten tips, and typically 0.3 nA for the current set point and 0.8 V for the sample bias voltage, V. This implies that we probed the unoccupied density of states (DOS) of PPMO. In order to check on the quality of the tunneling contacts the dependence of the tunneling current I on relative tip-sample distance z was repeatedly measured throughout the experiments. The exponential dependence of $I(z)$ yielded typical values of the effective work function $\Phi \sim 1.5$ eV confirming excellent vacuum tunnel barriers. Topography often showed terraces with step heights (~0.4 nm) close to the unit cell extension which indicates a $\langle 100 \rangle$ surface of the pseudocubic perovskite crystal.

To map the surface electronic state, we carried out thousands of STS measurements at 30 K $\leq T \leq$ 300 K and—for each T—at different locations on the sample surface. Typically, an area of 50 $\times$ 50 nm^2 with a lateral resolution of 1 nm (2500 pixels) was investigated. Tunneling current I and differential conductance, $G = dI/dV$, were measured simultaneously while ramping V from –1 to +1 V. An average of 2500 G-V curves taken at representative T are shown in Fig. 2(a). At $T < T_{MI} \approx$ 255 K, the G-V curves display metallic behavior with a finite value of G_0 signifying a finite DOS at the Fermi energy E_F. In contrast, at 300 K the G-V curve around $V = 0$ is indicative of a semiconducting gap. The strong asymmetry of the G curves at $T \lesssim T_{MI}$ and their severe change beyond T_{MI} point at a strongly modified DOS at T_{MI}.

For quantifying the STS results and their temperature evolution, the *local* G_0 is presented in color-coded conductance maps, Fig. 2(b)–(e), with the color scale covering $0 \leq G_0 \leq 0.64$ nS. These conductance maps represent slopes of individual I–V curves at $V \rightarrow 0$. The homogeneity of the local
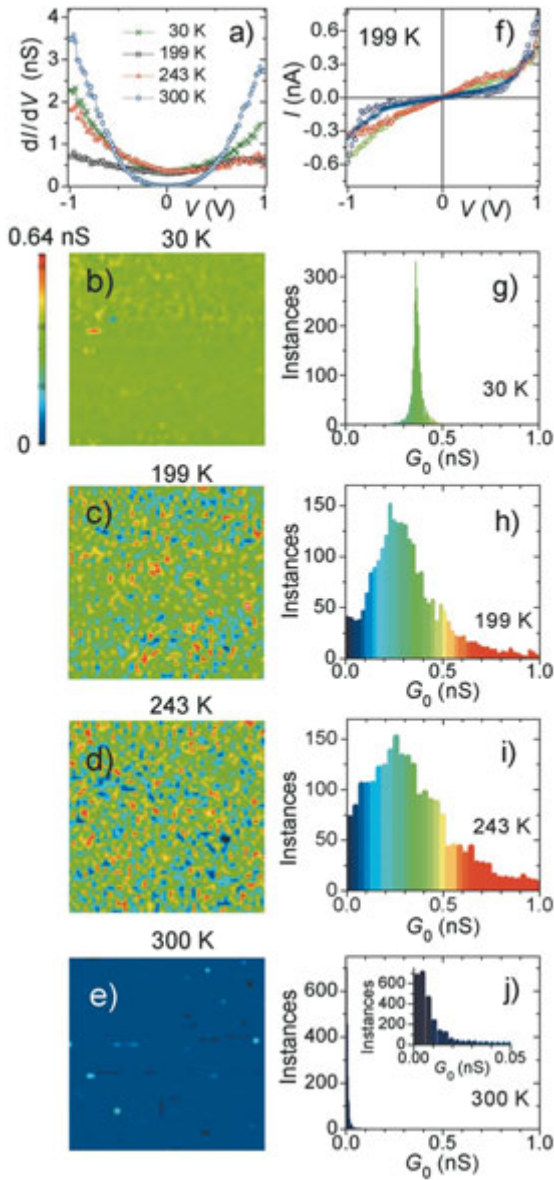
Fig. 2: (a) G-V curves averaged over 50 × 50 nm² at 30, 199, 243 and 300 K indicating metallic (T < T_{MI} ≈ 255 K) and insulating behavior. (b)–(e) Maps (50 × 50 nm²) of the local zero-bias conductance G_0 for the same T, i.e. through T_C and T_{MI}. The color encodes the value of G_0, see (b). (f) I-V curves taken at different positions at 199 K. (g)–(j) Histograms of G_0 for the maps (b)–(e) using the same color code. Inset to (j): zoom into the low G_0 regime.

DOS at E_F can be inferred from the corresponding histograms, Fig. 2(g)–(j), presenting the frequency of the observed G_0 values within the conductance maps in the same color code. A sharp distribution of G_0 at 30 K confirms a homogeneous electronic phase at low $T < T_C$. Similarly, the conductance map at 300 K (in the insulating regime) is also highly homogeneous [Fig. 2(e)], with most of the G_0 values very close to zero [Fig. 2(j) and inset].

Observation of phase separation

Interestingly, as T is raised through T_C and approaches T_{MI} ≈ 255 K inhomogeneities start to develop at a length scale of 2–3 nm, as seen in Fig. 2(c) and (d). A few of the I–V curves taken at T = 199 K are shown in Fig. 2(f). These curves reveal both metallic and insulating behavior at different points on the surface. A bimodal distribution of G_0 at 199 K is clearly visible in Fig. 2(h), with two maxima in G_0 frequency located at similar G_0-values as for low and high T, respectively. The increasing weight at G_0→0 while retaining a peak at G_0 ≈ 0.3 nS provides a direct observation of coexisting insulating and conducting regions and hence, nanometer-scale PS as well as growth of the former with T. Importantly, unlike reported previously [5,6], this PS does *not* persist deep into the ferromagnetic state in this compound. At T < 177 K, no indication of the insulating phase is found. Notably, this temperature coincides with the onset of constancy in $(d\rho/dT)/(\rho/T)$ below the dip near T_C (red dashed line in Fig. 1).

In Fig. 3, the G_0 values (green crosses) of the main peak in the histograms are plotted in dependence on temperature. This peak shifts to lower conductance values as T is increased and, importantly, an increasing weight at G_0→0 is observed for $T \geq 199$ K. The existence of a finite number of instances with $G_0 \cong 0$, *i.e.* of insulating areas, at and above 199 K is marked by blue triangles in Fig. 3. We observe a drastic change in the G_0 distribution when cooling below 260 K: the conducting areas appear then to immediately dominate the histograms. This temperature coincides with the rapidly changing bulk property $\rho(T)$ near T_{MI} [Fig. 3] which indicates that our STS results are *not dominated* by surface effects.

However, the distributions near T_{MI} [*cf.* Fig. 2(h), (i)] are significantly broadened compared to both, low T (30 K) and high T = 300 K > T_{MI}. The sharp distribution at T = 300 K clearly indicates that these broad distributions of G_0 at intermediate T reflect a sample property rather than an instrumental influence. The T dependences observed in STS arise mainly from a strongly changing DOS of PPMO at these temperatures. This change of electronic properties can be explained by the release of lattice distortions around T_{MI}, when immobilized polaronic carriers become successively mobile producing spatially inhomogene-
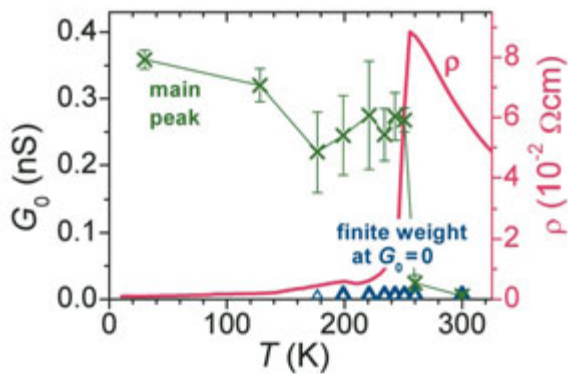
Fig. 3: G_0-value (×, green) of the main peak in the histograms vs. T. Error bars indicate the spread for multiple STS measurements. Triangles (blue) mark the presence of a finite number of instances with $G_0 = 0$, i.e. of insulating areas. $\rho(T)$ is plotted (pink line, right scale) to show the agreement of surface and bulk measurements.

ous conductance distributions. The positive temperature coefficient of resistance observed above T_C can be explained by electronic transport through percolating metallic regions. Moreover, the inhomogeneities due to PS may directly influence the DOS on a local scale: the DOS of nanometer-size particles is known to be modified with respect to the bulk.

By comparing topography and conductance maps taken over identical areas we could exclude that the PS is directly correlated with topography. Moreover, scans over areas of 20×20 nm^2 with a lateral resolution of 0.4 nm exhibit similar sizes of the individual phases as in the case of 50×50 nm^2 scans. Non-identical trace and retrace maps reveal a slow glassy dynamics of the electronic states and confirm that the PS observed here is not due to static chemical disorder.

Our findings are distinct from previous experimental results where PS was seen on a (sub-) micrometer scale and persisted deep into metallic regime. It remains an open question, whether the particular properties of PPMO with a metallic paramagnetic state for $T_C \lesssim T < T_{MI}$ are responsible for the clear observation of nanometer-scale phase separation and its confinement to this temperature range, and whether the result can be generalized to other mixed valence manganites. Further, the specific pattern of electronic inhomogeneity in the local surface DOS is certainly affected by unavoidable intrinsic disorder, induced by random chemical substitutions and/or surface

effects. In addition, disorder effects due to size differences between A-site Pr^{3+} and Pb^{2+} ions may play a role. However, the observed nanometer-scale PS is not a simple and fixed result of static chemical disorder, as can be inferred from the homogeneity of the electronic properties deep in the metallic state (low T) as well as in the insulating one (300 K). Therefore, in order to resolve the relevance of disorder effects on PS and the associated length scale, similar spatially resolved STS studies on different manganites are called for.

References

[1] *Y. Tokura (ed.)* "Colossal Magnetoresistive Oxides" (Gordon and Breach, Amsterdam, 2000).

[2] *J. M. D. Coey, M. Viret and S. von Molnár,* Adv. Phys. **48** (1999) 167.

[3] *E. Dagotto* "Nanoscale phase separation and colossal magnetoresistance" (Spinger, Heidelberg, 2002).

[4] *M. Uehara, S. Mori, C. H. Chen, and S.-W. Cheong,* Nature **399** (1999) 560.

[5] *M. Fäth, S. Freisem, A. A. Menovsky, Y. Tomioka, J. Aarts, J. A. Mydosh,* Science **285** (1999) 1540.

[6] *T. Becker et al,* Phys. Rev. Lett. **89** (2002) 237203.

[7] *L. Zhang et al.,* Science **298** (2002) 805.

[8] *D. D. Sarma et al.,* Phys. Rev. Lett. **93** (2004) 097202.

[9] *A. L. Malvezzi, S. Yunoki, and E. Dagotto,* Phys. Rev. B **59** (1999) 7033.

[10] *A. Moreo, S. Yunoki, and E. Dagotto,* Science **283** (1999) 2034.

[11] *A. Moreo et al.,* Phys. Rev. Lett. **84** (2000) 5568.

[12] *V. Moshnyaga et al.,* Phys. Rev. Lett. **97** (2006) 107205.

[13] *C. Israel, M. J. Calderon, and N. D. Mathur,* Materials Today **10** (2007) 24.

[14] *M. Paranjape et al.,* Phys. Rev. B **67** (2003) 214415.

[15] *Ch. Renner and H. M. Rønnow,* in Scanning Probe Microscopy: Electrical and Electromechanical Phenomena at the Nanoscale, ed. S. Kalinin (Spinger, Berlin, 2006).

[16] *B. Padmanabhan et al.,* J. Magn. Magn. Mater. **307** (2006) 288.

[17] *B. Padmanabhan et al.,* Phys. Rev. B **75** (2007) 024419.

[18] *R.-W. Li et al.,* Phys. Rev. B **71** (2005) 092407.

[19] *J. M. DeTeresa et al.,* Nature **386** (1997) 256.

[1] Department of Physics, Indian Institute of Science, Bangalore 560012, India